中國機械工程學刊第四十一卷第五期第 671~680 頁(民國一百零九年)
Journal of the Chinese Society of Mechanical Engineers, Vol.41, No.5, pp 671~680 (2020)

Workspace and Singularity Analysis of a 3-P$\bar{\text{R}}\bar{\text{R}}$S Parallel Robot

Amnad Tongtib* and Theeraphong Wongratanaphisan**

Keywords: Parallel robot, Workspace, Singularity, Grassmann-Cayley Algebra

ABSTRACT

This paper presents in-depth kinematic, workspace and singularity analysis of a six-degree-freedom parallel robot having 3-P$\bar{\text{R}}\bar{\text{R}}$S structure. The robot has three identical link chains connected together by a triangular moving platform. Each link chain composes of three rigid bodies connected by two actuating revolute joints. These link chains are connected to base with passive prismatic joint and to the moving platform by passive spherical joints. Explicit inverse kinematic solutions are provided and forward kinematic solutions are determined by dialytic elimination technique. Through its special structure, geometrical method for finding three types of workspace (constant orientation, reachable and dexterous) are given. By using Grassmann-Cayley Algebra, planes can be formed geometrically to determine singularity configurations of the robot. The method presented is advantageous as it provides geometrical insight to singularity conditions which help to avoid their occurrence in the design stage.

INTRODUCTION

Robot manipulator design is one the topics that has attracted researchers all over the world. Mainly, there are two types of robot structure: serial and parallel. Serial robot is an open chain of links connected in series with one link connected to ground. This open chain structure inherits large workspace with high degree of freedom (DOF). However, the structural stiffness of this type of robot is low and hence cannot operate at high bandwidth. Parallel robots, on the other hand, have more than one links connected to ground. Due to its parallel structure, parallel robots have higher stiffness and are more accurate than the serial counterpart.

For parallel robots, inverse kinematic solutions can be found straightforwardly. Forward kinematic solutions, however, are more difficult to solve. There are 3 approaches to obtain solutions for forward kinematic: closed-form analysis, numerical technique and analytical technique. The closed-form solutions of forward kinematic may be determined for parallel robots with special structure. For example, the structure of Gough platform (Ping and Houngtao, 2001; Kai, Fitzgerald and Lewis, 1993; Xiguang and Guangping, 2009) are symmetrically arranged such that the solutions resolve into closed-form. For most other parallel robots, closed-form solutions do not exist. Most forward kinematic relations are in the form of a set of nonlinear equations which are solved simultaneously by numerical techniques. The method such as Newton-Raphson (Melet, 2006) and Global Newton Raphson (Chifu et al., 2009) have been shown to effectively obtain the solutions. However, for some special structure, the form of equations can be arranged into polynomial equations which is referred as analytic form. Then, in this case, the solutions can be solved using standard techniques such as dialytic elimination method (Tsai, 1999; Chen, et al., 2012; Tongtib, et al., 2016).

In robot design, workspace is one of the main topics to consider. Generally, there are four main types of workspace (Gosselin, 1990; Merlet, 1999): 1) Constant orientation workspace 2) Orientation workspace 3) Inclusive orientation workspace 4) Total orientation workspace. There are mainly two approaches to obtain the workspace of a robot: numerical and geometrical. In the numerical approach, the area/volume in the scope of interest is divided into grids of data points. All data points will be checked with kinematic equations of the robot. For each data point, if the constraints are satisfied, it is then located in the workspace. This technique is simple and accurate but it is numerical intensive. On the other hand, for some structures, geometrical approach (Gosselin, 1990; Merlet, 1999) can determine the workspace with less calculation. This geometrical approach has advantages in that it gives preliminary idea of how the workspace will look like before entering into the calculation.

Paper Receivedr November, 2018. Revised December, 2018. Accepted February, 2019. Author for Correspondence: Theeraphong Wongratanaphisan

Ph. D student, Graduate Program, Department of Mechanical Engineering, Chiang Mai University, Chiang Mai, Thailand, 50200

**Associate Professor, Department of Mechanical Engineering, Chiang Mai University, Chiang Mai, Thailand, 50200*

Singularities may exist at the boundary as well as inside of the robot's workspace. At singularity configurations, the robot losses either its degree of freedom or controllability depending on type of singularity. The singularity can be analyzed from the velocity transformation matrix between inputs and outputs (Gosselin and Angels, 1990) called the "Jacobian" matrix. Both numerical and geometrical approaches have been used to find the singularity configurations. For numerical method, e.g. in Qian et al., (2013), the ranks of the Jacobian matrices for all tested positions in the workspace are checked. The position at which the rank of the Jacobian matrix is deficit reflects the singular position. For geometrical approach, imaginary lines and planes formed from the passive joints of the robot are used to describe the singular configurations (see Ben-Horin and Shoham, 2006; Monsarrat and Gosselin, 2001; Kefei et al., 2017). The advantage of this approach is that it gives visual information which can be used to analyze the structure of the robot in early stage of design.

Although, parallel robots have desirable advantages in higher stiffness, more accurate and low inertia, its drawbacks are also significant in terms of workspace and singularity. The number of legs in parallel robot plays an important role in limiting the size of the workspace. For example, a popular 6-DOF Stewart platform has six legs causing its workspace to be very small. In this study, we aim to design a 6-DOF parallel robot that has larger workspace by employing a three-leg structure with 3-P$\overline{\text{R}}\overline{\text{R}}$S configuration. To the best of our knowledge, in-depth kinematic analysis, workspace and singularity of this type of structure have not been covered elsewhere and this paper aims to make this contribution.

The remainder of the paper is organized as follows. Section 2 presents the description and kinematic analysis of 3-P$\overline{\text{R}}\overline{\text{R}}$S parallel robot. In Section 3, the workspace determination will be explained. The procedure to obtain dexterous, reachable and constant orientation workspaces will be covered. In Section 4, the singularity conditions of this robot are analyzed using geometrical technique based on Grassmann-Cayley Algebra. Finally, conclusions are provided in Section 5.

A 3-P$\overline{\text{R}}\overline{\text{R}}$S PARALLEL ROBOT

Description

Figure 1 (a) shows the schematic diagram of a 3-P$\overline{\text{R}}\overline{\text{R}}$S parallel robot. The robot consists of a mobile platform shown as a triangle plate connected to a fixed base with three P$\overline{\text{R}}\overline{\text{R}}$S link chains. Each link chain consists of three rigid bodies connected serially by two actuating revolute joints. They are connected to the mobile platform with passive spherical joints and connected to a fixed base by passive prismatic joints. Each link chain operates on a plane that can translate along a fixed perpendicular axis. Link-chain 1 lies on the Y-Z plane and moves along the X-axis. Similarly, Link-chain 2 operates on the X-Z plane that can translate along the Y-axis and Link-chain 3 operates in the X-Y planes that can translate along the Z-axis. The end of each link chain is connected to the triangular moving platform by a passive spherical joint at D_n, n=1,2,3. The coordinates of D_ns are denoted by (X, D_{y1}, D_{z1}), (D_{x2}, Y, D_{z2}) and (D_{x3}, D_{y3}, Z), respectively where X, Y and Z are passive positions along X-axis, Y-axis and Z-axis, respectively.

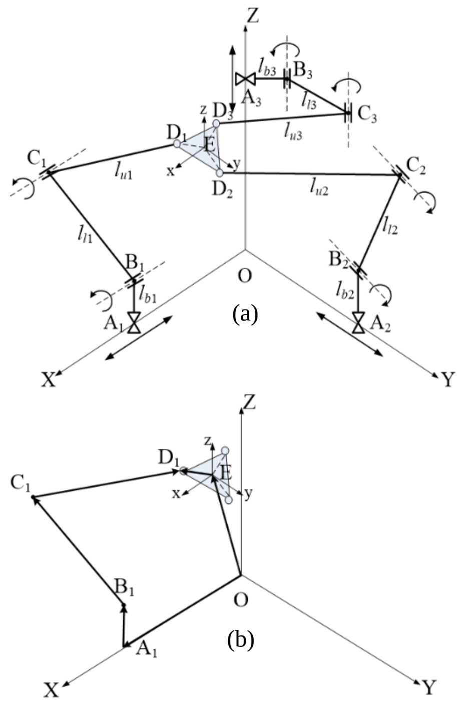

Fig. 1. (a) Schematic description of a 3- P$\overline{\text{R}}\overline{\text{R}}$S parallel robot; (b) vector loop of Link-chain 1.

The degree of freedom)mobility number (of this robot can be determined by

$$M=6(n-1)-5f_1-4f_2-3f_3, \tag{1}$$

where

M = degree of freedom (D.O.F.)
n = number of links (including the base)
f_i = number of joint with i D.O.F.

Here, n=11, f_1 = 9, f_2 = 0 and f_3 = 3. Therefore, the robot has 6 degrees of freedom which allows it to perform tasks that require positioning and orientating an object in three-dimensional space.

Kinematic of a 3-P$\overline{\text{R}}\overline{\text{R}}$S parallel robot

In Fig. 1 (b), let O(0,0,0) be the origin of the fixed frame and E(e_x,e_y,e_z) be the origin of the x-y-z frame which is attached to the moving platform. Let R be the rotation matrix which maps the moving x-y-z frame onto the fixed X-Y-Z frame. The basic rotation matrices about X, Y and Z-axes are given as

$$R_X(\theta_X)=\begin{bmatrix}1 & 0 & 0\\ 0 & \cos\theta_X & -\sin\theta_X\\ 0 & \sin\theta_X & \cos\theta_X\end{bmatrix}, R_Y(\theta_Y)=\begin{bmatrix}\cos\theta_Y & 0 & -\sin\theta_Y\\ 0 & 1 & 0\\ -\sin\theta_Y & 0 & \cos\theta_Y\end{bmatrix},$$

$$R_Z(\theta_Z)=\begin{bmatrix}\cos\theta_Z & -\sin\theta_Z & 0\\ \sin\theta_Z & \cos\theta_Z & 0\\ 0 & 0 & 1\end{bmatrix},$$

where θ_X, θ_Y and θ_Z are orientations of moving platform about X, Y and Z axes, respectively. The overall rotation matrix R can be determined by successive rotation operations about principal axes X, Y and Z and is given by

$$R=R_Z(\theta_Z)R_Y(\theta_Y)R_X(\theta_X). \tag{2}$$

For each link chain n:

$$\overline{OD_n}+R\overline{D_nE}=\overline{OE}. \tag{3}$$

Note that, $\overline{D_nE}$ are the known local distance vectors fixed in the rotating frame.

Inverse kinematic

When the position E and orientation of the moving platform, represented by the rotation matrix R, are given, the positions of all D_ns can be uniquely determined. For each link chain,

$$\overline{OD_n}=\overline{OE}-R\overline{D_nE}. \tag{4}$$

Each link chain can be considered as a 3-DOF serial planar manipulator with two actuators and one passive joint. Once the coordinate of D_n is determined, one can find the input joint angles of the actuators.

Figure 2 shows description of each link chain on a local r-s plane which is used to describe the planes X-Z, Y-Z and X-Y, respectively. The coordinate of D_n (D_{sn} and D_{tn}) associated with link n can be directly determined by forward kinematic of serial structure as:

$$D_{sn}=l_{ln}\cos\theta_{1n}+l_{un}\cos\theta_{2n} \tag{5}$$

$$D_{tn}=l_{ln}\sin\theta_{1n}+l_{un}\sin\theta_{2n} \tag{6}$$

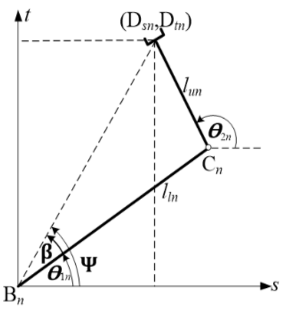

Fig. 2. Schematic description of each link chain.

From Eqs. (5) and (6), the inverse kinematic solutions of each link chain can be determined from:

$$\theta_{2n}=\theta_{1n}+\tan^{-1}\left(\pm\sqrt{1-{t_n}^2}/t_n\right), \tag{7}$$

$$\theta_{1n}=\tan^{-1}\left(\frac{D_{tn}}{D_{sn}}\right)-\tan^{-1}\left(\frac{l_{un}\sin(\theta_{2n}-\theta_{1n})}{l_{ln}+l_{un}\cos(\theta_{2n}-\theta_{1n})}\right), \tag{8}$$

where $t_n=\left(D_{sn}^2+D_{tn}^2-l_{ln}^2-l_{un}^2\right)/2l_{ln}l_{un}$.

Components D_{sn} and D_{tn} are the projections of point D onto the s-t plane in leg n. l_{ln} and l_{un} are the lengths of lower and upper segments of the link chain n. Note in Eqs. (7) and (8) that for a given pair of D_{y1} and D_{z1} there exist two solutions pairs of θ_{1n} and θ_{2n}. In inverse kinematic problem, X, Y and Z are variables that need not be determined directly. Their values will follow the constraints resulted from connecting the three link chains to the moving platform.

Forward kinematic

The opposite problem to the inverse kinematic is: given the six input variables θ_{11}, θ_{21}, θ_{12}, θ_{22}, θ_{13} and θ_{23}, then find the three coordinates of D_is which together can be used to solve for the position of the end-effector point E and the rotation matrix R. Note that D_{y1}, D_{z1}, D_{x2}, D_{z2} D_{x3}, D_{y3} can be directly determined from Eqs. (5)-(6). The remaining steps are to find X, Y and Z. These three variables are related through three following constraints:

$$\|D_1-D_2\|=d_1,\ \|D_2-D_3\|=d_2,\ \|D_1-D_3\|=d_3, \tag{9}$$

where d_1, d_2 and d_3 are the distances between corresponding points. Eq. (9) can be rearranged as

$$k_2X^2+k_1X+k_0=0, \tag{10}$$

$$m_2Y^2+m_1Y+m_0=0, \tag{11}$$

$$k_5Y^2+k_4Y+k_3=0, \tag{12}$$

where

$$k_0=-d_3^2+D_{x1}^2+D_{x2}^2-2D_{x2}D_{y2}+D_{y2}^2+Z^2-2ZD_{z2}+D_{z2}^2,$$

$$k_1=-2D_{x1},\ k_2=1,\ k_4=-2D_{x2}, k_5=1,\ m_1=-2D_{y2}, m_2=1,$$

$$k_3=-d_2^2+D_{x1}^2+D_{x2}^2-2D_{x1}D_{x3}+D_{x3}^2+Z^2-2ZD_{z3}+D_{z3}^2,$$

$$m_0=-d_1^2+D_{x3}^2+D_{y2}^2-2D_{z2}D_{z3}+D_{z3}^2+X^2-2XD_{x3}+D_{z3}^2.$$

Note that the coefficients k_0, k_3 are functions of Z, k_1, k_2, k_4, k_5, m_1, m_2 are constants and m_0 is a functions of X. Dialytic elimination method can be used to eliminate Y and X in Eqs. (10), (11) and (12), resulting in a function of 8th-order polynomial in Z:

$$\sum_{i=0}^{8} a_iZ^i=0, \tag{13}$$

where the coefficients a_i (i =0, 1, …, 8) are constants (the symbolic forms of a_i are shown in the Appendix). Note that the maximum number of possible solutions of Z is 8 (Tongtib, et.al. 2016). Once the solutions for Z are obtained, X can be directly calculated from Eq. (10) and Y can be obtained from Eq. (11) or (12). Note that for each value of Z, two real values (if exists) of X and two real values (if exists) of Y can be obtained.

WORKSPACE ANALYSIS

For the 3- $\mathrm{P\bar{R}\bar{R}S}$ parallel robot, the reachable workspace can be visually observed as an intersection of the working volumes of three link chains. The working volumes of these link chains are seen as tubes along X, Y and Z axes for Link-chain 1, 2 and 3, respectively (See Fig. 3).

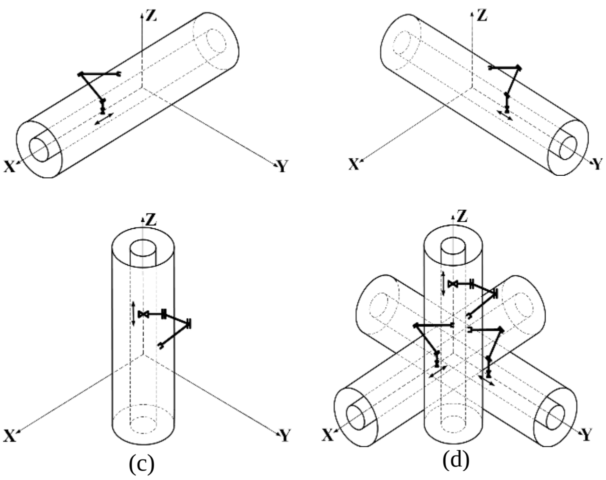

Fig. 3. The tube-shape working volume of (a) Link-chain 1; (b) Link-chain 2; (c) Link-chain 3; (d) three link chains.

Constant orientation workspace

The constant orientation workspace is a three-dimensional space in which the end-effector can reach when the orientation of moving platform is held fixed. For the 3- P$\overline{\text{RR}}$S parallel robot, the constant orientation workspace is determined by intersection of working volume of each link chain. For Link-chain 1, the working volume is confined between two surfaces represented by outer and inner cylindrical equations along X-axis:

$$(y\text{-}y_1)^2+(z\text{-}z_1)^2=(l_{l1}+l_{u1})^2, \tag{14}$$

$$(y'\text{-}y_1)^2+(z'\text{-}z_1)^2=(l_{l1}\text{-}l_{u1})^2. \tag{15}$$

The working volume of Link-chain 2 and Link-chain 3 can be obtained similarly:

$$(x\text{-}x_2)^2+(z\text{-}z_2)^2=(l_{l2}+l_{u2})^2, \tag{16}$$

$$(x'\text{-}x_2)^2+(z'\text{-}z_2)^2=(l_{l2}\text{-}l_{u2})^2, \tag{17}$$

$$(x\text{-}x_3)^2+(y\text{-}y_3)^2=(l_{l3}+l_{u3})^2, \tag{18}$$

$$(x'\text{-}x_3)^2+(y'\text{-}y_3)^2=(l_{l3}\text{-}l_{u3})^2\ . \tag{19}$$

Here, x_n y_n and z_n are the effective centers of the circle which are dependent on the orientation of the mobile platform. The workspace is considered first individually for each leg. For Link- chain 1 and Link-chain 2, they are cylindrical shape along x- and y-axes, respectively. As viewed in the X-Y plane, the workspace is determined by the intersection of two rectangles as shown in Fig. 4 (a). Fig. 4 (b) describes the intersection of the working area of Link-chain 1 and Link-chain 2. For Link-chain 3, the workspace is cylindrical shape along Z-axis.

Fig. 5 shows the boundary workspace of each link chain and the result of intersection of the boundaries on X-Y plane for example case of l_{ln}=600 mm, l_{un}=200 mm, l_{bn}=0 mm and d_n=110 mm (n=1, 2, 3) and orientations of moving platform (O_x,O_y,O_z)=(90º,0,0). Then, the working volume of this robot can be determined by intersection of these three volumes as shown in Fig. 6.

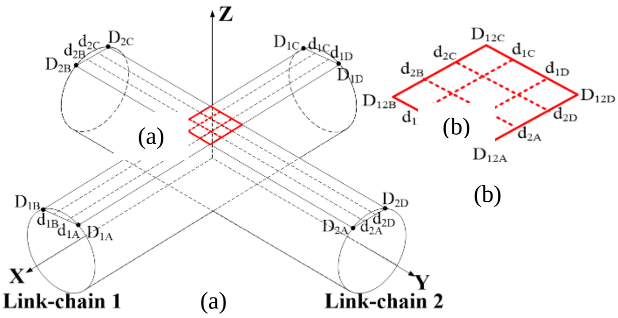

Fig. 4. (a) working volume of Link-chain 1 and Link-chain 2; (b) intersection of working volume on the X-Y plane.

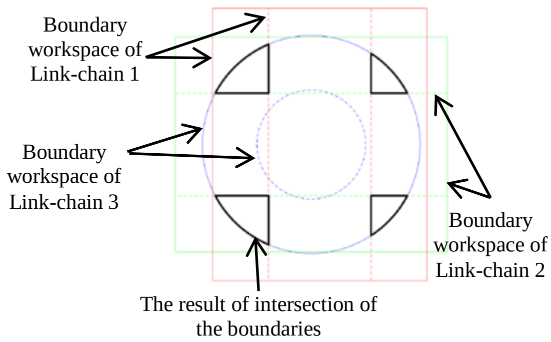

Fig. 5. Example of constant orientation workspace on X-Y plane (Z=100 mm).

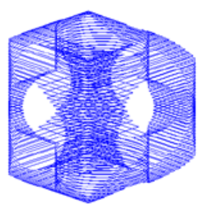

Fig. 6. The intersection of these three volumes forms a constant orientation workspace.

Reachable workspace

The reachable workspace consists of all locations of the end-effector that the robot can reach regardless of its orientation value. For this workspace, similar concept for determination of the constant orientation workspace can be used with the radius of the tube changed to $(l_{ln}+l_{un}+r_p)^2$ for outer cylinder and $(l_{ln}+l_{un}\text{-}r_p)^2$ for inner cylinder. Therefore, Eqs. (14) – (19) can be rewritten as

$$\begin{aligned} &y^2+z^2=(l_{l1}+l_{u1}+r_p)^2,\ y'^2+z'^2=(l_{l1}\text{-}l_{u1}\text{-}r_p)^2,\\ &x^2+z^2=(l_{l2}+l_{u2}+r_p)^2,\ x'^2+z'^2=(l_{l2}\text{-}l_{u2}\text{-}r_p)^2, \end{aligned} \tag{20}$$

$$x^2+y^2=\left(l_{l3}+l_{u3}+r_p\right)^2,\ x'^2+y'^2=\left(l_{l3}-l_{u3}-r_p\right)^2.$$

Here, r_p is the distance from the end-effector to the end-point of moving platform of each link chain.

Dexterous workspace

The dexterous workspace consists of all positions of the end-effector that the robot can reach with an arbitrary orientation. The radius of the tube in this workspace is $\left(l_{ln}+l_{un}-r_p\right)^2$ for outer cylinder and $\left(l_{ln}+l_{un}+r_p\right)^2$ for inner cylinder. Again, Eqs. (14) – (19) can be rewritten as:

$$\begin{aligned}
&y^2+z^2=\left(l_{l1}+l_{u1}-r_p\right)^2, y'^2+z'^2=\left(l_{l1}-l_{u1}+r_p\right)^2,\\
&x^2+z^2=\left(l_{l2}+l_{u2}-r_p\right)^2, x'^2+z'^2=\left(l_{l2}-l_{u2}+r_p\right)^2,\\
&x^2+y^2=\left(l_{l3}+l_{u3}-r_p\right)^2, x'^2+y'^2=\left(l_{l3}-l_{u3}+r_p\right)^2.
\end{aligned} \tag{21}$$

Fig. 7 compares the three workspaces in a selected cross section near the center of the workspace and Fig. 8 compares the three working volumes of a 3-$\text{P}\bar{\text{R}}\bar{\text{R}}\text{S}$ parallel robot. Clearly, the size of reachable workspace is the biggest and that of the dexterous workspace is the smallest. However, the workspace of the 3-$\text{P}\bar{\text{R}}\bar{\text{R}}\text{S}$ parallel robot is generally bigger than the well-known Stewart platform.

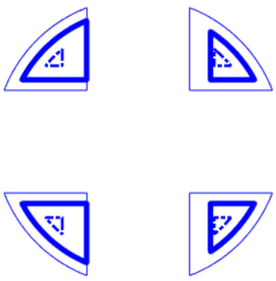

Fig. 7. Three types workspace on the plane: reachable workspace (solid line), constant orientation workspace (bold solid line), dexterous workspace (dashed lines) at Z=100 mm.

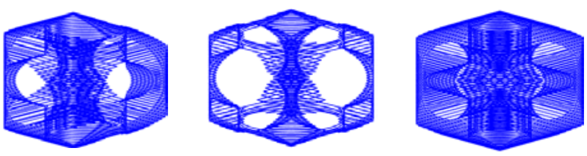

(a) Constant orientation workspace | (b) Dexterous workspace | (c) Reachable workspace

Fig. 8. Comparison three types working volume.

SINGULARITY ANALYSIS

The singularity condition reflects the configurations that the robot cannot provide motion in the workspace because either the degree of freedom is degenerated or the robot geometrically loses controllability. At these configurations, the robot cannot transmit force or torque to the end-effector to generate velocity. The singularity conditions relate to degeneracy of Jacobian matrix. One can numerically, check the rank of the Jacobian matrix at each position to test the singularity of that position.

Jacobian of the 3-$\text{P}\bar{\text{R}}\bar{\text{R}}\text{S}$ parallel robot

The Jacobian matrix J is a transformation matrix between joint velocities and task velocities. The velocity kinematics of a parallel robot can be written as:

$$A\dot{X}=B\dot{q}, \tag{22}$$

$$\dot{q}=J\dot{X} \tag{23}$$

where $J=B^{-1}A$ (see Tsai, 1999). Here $\dot{X}$ is the vector containing task velocities and $\dot{q}$ is the vector of joint velocities. A and B are the Jacobian matrices related to task velocities and joint velocities, respectively. Let us define the following notations: $q=[\theta_{11}\theta_{21}\theta_{12}\theta_{22}\theta_{13}\theta_{23}]^T$ are the of the joint variables, $X=[x\ \ y\ \ z\ \ \theta_x\ \ \theta_y\ \theta_z]^{\mathrm{T}}$ are of the end-effector pose variables, $W=[F_x\ \ F_y\ \ F_z\ \ M_x\ \ M_y\ \ M_z]^{\mathrm{T}}$ are the forces and moments of the end-effector, and $\tau=[\ \tau_{11}\ \ \tau_{21}\ \ \tau_{12}\ \ \tau_{22}\ \ \tau_{13}\ \ \tau_{23}]^{\mathrm{T}}$ are the actuator torques. By force-velocity duality principle, the Jacobian matrix can also be determined from the relation:

$$W=J^T\tau \tag{24}$$

where W is a wrench (forces and moments) acting on the end-effector. Define r_n-s_n-t_n as local frame attached to link n (see Fig. 9).

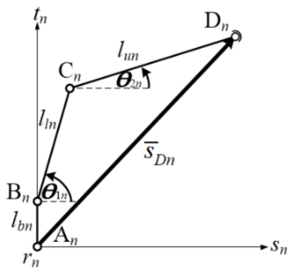

Fig. 9. Vectors related to link n in local r_n-s_n-t_n frame.

The position of D_n is in r_n-s_n-t_n frame is related to the actuating joint variables θ_{1n} and θ_{2n} by

$$\bar{s}_{Dn}=\begin{bmatrix}0\\0\\l_{bn}\end{bmatrix}+l_{ln}\cdot\begin{bmatrix}0\\\cos\theta_{1n}\\\sin\theta_{1n}\end{bmatrix}+l_{u1}\cdot\begin{bmatrix}0\\\cos\theta_{2n}\\\sin\theta_{2n}\end{bmatrix}+\begin{bmatrix}L_n\\0\\0\end{bmatrix} \tag{25}$$

where L_n is the passive prismatic distance from the origin of X-Y-Z frame. The torques from actuators in each link chain n transfer effective force $f_{Dn}=[f_{Dn,x}, f_{Dn,y}, f_{Dn,z}]^{\mathrm{T}}$ through these D_n points (see Fig. 10) to the end-effector to generate task-space wrench W. Consider attaching local frame r-s-t to each link chain as follow: Link-chain 1 – r, s, t are aligned with X,Y, Z axes, respectively; Link-chain 2 – r, s, t are aligned with Y, Z, X axes, respectively; Link-chain 3 – r, s, t are aligned with Z,Y, X axes, respectively. At equilibrium, the virtual work principle applies:

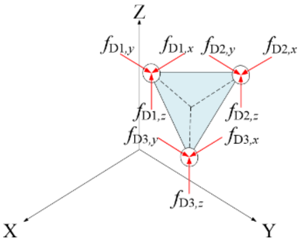

Fig. 10. Forces acting on spherical joints.

$$\delta w=\textstyle\sum_{n=1}^{3}\sum_{j=1}^{2}\tau_{jn}\delta\theta_{jn}+\sum_{n=1}^{3}(f_{Dn}\delta\bar{s}_{Dn})=0 \qquad (26)$$

Note that the wrench $W=[F\ M]^T$ relates to f_{Dn} by

$$F=\textstyle\sum_{n=1}^{3}f_{Dn}=\sum_{n=1}^{3}\sum_{j=1}^{2}\tau_{jn}v_{jn} \qquad (27)$$

$$M=\textstyle\sum_{n=1}^{3}(R\cdot\overline{ED}_n)\times f_{Dn}=\sum_{n=1}^{3}\sum_{j=1}^{2}\tau_{jn}(R\cdot\overline{ED}_n\times v_{jn}) \qquad (28)$$

where R is the rotation matrix from x-y-z frame to X-Y-Z frame, from Eq. (2), and

$$v_{11}=\frac{1}{l_{l1}\sin(\theta_{21}\text{-}\theta_{11})}\begin{bmatrix}0\\ \text{-}\cos\theta_{21}\\ \text{-}\sin\theta_{21}\end{bmatrix},\ v_{21}=\frac{1}{l_{u1}\sin(\theta_{21}\text{-}\theta_{11})}\begin{bmatrix}0\\ \cos\theta_{11}\\ \sin\theta_{11}\end{bmatrix},$$

$$v_{12}=\frac{1}{l_{l2}\sin(\theta_{12}\text{-}\theta_{22})}\begin{bmatrix}\cos\theta_{22}\\ 0\\ \text{-}\sin\theta_{22}\end{bmatrix},\ v_{22}=\frac{1}{l_{u2}\sin(\theta_{12}\text{-}\theta_{22})}\begin{bmatrix}\text{-}\cos\theta_{12}\\ 0\\ \sin\theta_{12}\end{bmatrix},$$

$$v_{13}=\frac{1}{l_{l3}\sin(\theta_{23}\text{-}\theta_{13})}\begin{bmatrix}\text{-}\cos\theta_{23}\\ \text{-}\sin\theta_{23}\\ 0\end{bmatrix},\ v_{23}=\frac{1}{l_{u3}\sin(\theta_{23}\text{-}\theta_{13})}\begin{bmatrix}\cos\theta_{13}\\ \sin\theta_{13}\\ 0\end{bmatrix}.$$

Hence from Eqs. (27) and (28)

$$\begin{bmatrix}F_x\\F_y\\F_x\\M_x\\M_y\\M_z\end{bmatrix}=\begin{bmatrix}v_{11} & v_{21} & v_{12} & v_{22} & v_{13} & v_{23}\\ R\cdot\overline{ED}_1\times v_{11} & R\cdot\overline{ED}_1\times v_{21} & R\cdot\overline{ED}_2\times v_{12} & R\cdot\overline{ED}_2\times v_{22} & R\cdot\overline{ED}_3\times v_{13} & R\cdot\overline{ED}_3\times v_{23}\end{bmatrix}\begin{bmatrix}\tau_{11}\\ \tau_{21}\\ \tau_{12}\\ \tau_{22}\\ \tau_{13}\\ \tau_{23}\end{bmatrix},$$

but

$$\begin{bmatrix}v_{11}^T & (R\cdot\overline{ED}_1\times v_{11})^T\\ v_{21}^T & (R\cdot\overline{ED}_1\times v_{21})^T\\ v_{12}^T & (R\cdot\overline{ED}_2\times v_{12})^T\\ v_{22}^T & (R\cdot\overline{ED}_2\times v_{22})^T\\ v_{13}^T & (R\cdot\overline{ED}_3\times v_{13})^T\\ v_{23}^T & (R\cdot\overline{ED}_3\times v_{23})^T\end{bmatrix}=\begin{bmatrix}\frac{1}{b_{11}} & 0 & 0 & 0 & 0 & 0\\ 0 & \frac{1}{b_{21}} & 0 & 0 & 0 & 0\\ 0 & 0 & \frac{1}{b_{12}} & 0 & 0 & 0\\ 0 & 0 & 0 & \frac{1}{b_{22}} & 0 & 0\\ 0 & 0 & 0 & 0 & \frac{1}{b_{13}} & 0\\ 0 & 0 & 0 & 0 & 0 & \frac{1}{b_{23}}\end{bmatrix}\begin{bmatrix}n_{11}^T & (R\cdot\overline{ED}_1\times n_{11})^T\\ n_{21}^T & (R\cdot\overline{ED}_1\times n_{21})^T\\ n_{12}^T & (R\cdot\overline{ED}_2\times n_{12})^T\\ n_{22}^T & (R\cdot\overline{ED}_2\times n_{22})^T\\ n_{13}^T & (R\cdot\overline{ED}_3\times n_{13})^T\\ n_{23}^T & (R\cdot\overline{ED}_3\times n_{23})^T\end{bmatrix}$$

where

$$\begin{aligned}&b_{11}=l_{l1}\sin(\theta_{21}\text{-}\theta_{11}),\ b_{21}=l_{u1}\sin(\theta_{21}\text{-}\theta_{11})\\ &b_{12}=l_{l2}\sin(\theta_{12}\text{-}\theta_{22}),\ b_{22}=l_{u2}\sin(\theta_{12}\text{-}\theta_{22})\\ &b_{13}=l_{l3}\sin(\theta_{23}\text{-}\theta_{33}),\ b_{23}=l_{u3}\sin(\theta_{23}\text{-}\theta_{33})\end{aligned} \qquad (29)$$

and

$$\begin{aligned}&n_{11}=l_{l1}\sin(\theta_{21}\text{-}\theta_{11}),\ v_{11}=\text{-}R_x(\theta_{21})\bar{j},\\ &n_{21}=l_{u1}\sin(\theta_{21}\text{-}\theta_{11}),\ v_{21}=R_x(\theta_{11})\bar{j},\\ &n_{12}=l_{l2}\sin(\theta_{12}\text{-}\theta_{22}),\ v_{12}=R_y(\theta_{22})\bar{k},\\ &n_{22}=l_{u2}\sin(\theta_{12}\text{-}\theta_{22}),\ v_{22}=\text{-}R_y(\theta_{12})\bar{k},\\ &n_{13}=l_{l3}\sin(\theta_{23}\text{-}\theta_{13}),\ v_{13}=\text{-}R_z(\theta_{23})\bar{i},\\ &n_{23}=l_{u3}\sin(\theta_{23}\text{-}\theta_{13}),v_{23}=R_z(\theta_{13})\bar{i}.\end{aligned} \qquad (30)$$

From Eqs. (22) and (24), A and B in can then be expressed by:

$$A=\begin{bmatrix}n_{11}^T & R\cdot\overline{ED}_1\times n_{11}^T\\ n_{21}^T & R\cdot\overline{ED}_1\times n_{21}^T\\ n_{12}^T & R\cdot\overline{ED}_2\times n_{12}^T\\ n_{22}^T & R\cdot\overline{ED}_2\times n_{22}^T\\ n_{13}^T & R\cdot\overline{ED}_3\times n_{13}^T\\ n_{23}^T & R\cdot\overline{ED}_3\times n_{23}^T\end{bmatrix}, \qquad (31)$$

$$B=\mathrm{diag}(b_{11},b_{21},b_{12},b_{22},b_{13},b_{23}). \qquad (32)$$

Singularity condition

The singularity condition can be analyzed from the property of matrices A and B. For parallel robot, there are three types of singularities. The first type occurs when the determinant of A approaches zero. This is when the end-effector is locally movable even all the actuators are locked. Thus, the robot is uncontrollable. The second type occurs when the determinant of matrix B approaches zero. At this instance, the actuator motion does not affect the motion of the end-effector in some directions/

orientations. The third type occurs when the first and second types occur simultaneously. There are generally two methods for determining singularity condition of a robot: numerical approach and geometry approach. The numerical approach is straightforward. The configuration space is divided into grids of input variables. The configuration variables in those grid points are then substituted into Eqs. (31) and (32) to obtain numerical value of the Jacobian matrix. If the rank of the Jacobian matrix is not full, then that configuration is singular. This approach is simple but computationally intensive. Furthermore, the method does not provide geometrical insight that one can use to avoid singularity condition at the design stage. The geometrical approach proves to be more useful for design purpose.

Grassmann-Cayley Algebra (Monsarrat and Gosselin, 2001) can be used to geometrically analyze these singularities in terms of arrangement of lines and planes. These lines are represented by Plucker vectors. For each leg, two of these vectors form a plane of action by local actuators. For the 3-P$\overline{R}\overline{R}$S parallel structure, from Eqs. (29) and (30), there are six unit vectors that represent these lines. For example, n_{11} and n_{21} represent the lines that belong to Link-chain 1.

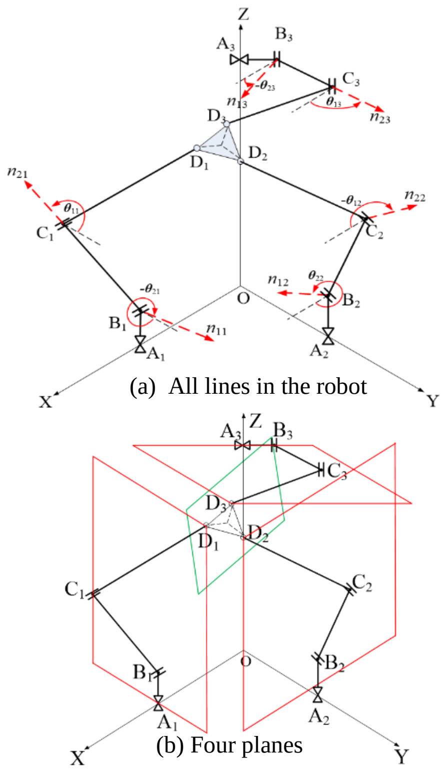

Fig. 11. Plane formed from Plucker vectors.

Fig. 11 (a) shows these six lines that belong to all three legs. The plane for Link-chain 1 is perpendicular to the x-axis. For Link-chain 2 and Link-chain 3, the planes are perpendicular to Y-axis and Z-axis, respectively (see Fig. 11 (b)). There is an additional plane which is formed from vector connecting three passive spherical joints of the moving platform. Therefore, there are a total of four planes.

The singularity can be analyzed from the arrangement of these planes using Grassmann-Cayley Algebra. There are five cases of singularity condition that relate to these four planes. The singularity occurs when(1) all four planes intersects at a common point; (2) two or more planes are coplanar; (3) three or more planes intersect along a common line; (4) one of the planes degenerates into a line; (5) one of the planes degenerates into a point.

Note that, case (4) and (5) will not occur because, due to its structure, the planes of this robot cannot degenerate to a line or a point. Therefore, only cases (1), (2) and (3) need to be considered. Figs. 12-14 show the configuration at which the singularity occur. In Fig. 12, three planes of Link-chain 1, Link-chain 2 and the plane of moving platform intersect along a common line (dashed line). In this configuration, two of the moving platform end points (in this case D_1 and D_2) will be on the intersection line. In this case, even when all the actuator joints are locked the moving platform will not be able to resist external moments that have component in the vertical direction (D_1D_2). In other words, at this instance D_3 can still infinitesimally rotates about line D_1D_2.

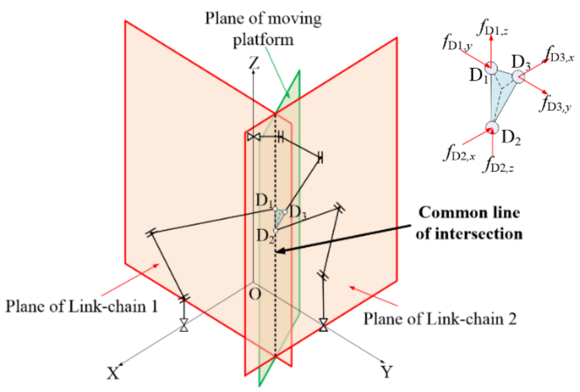

Fig. 12. First type of singularity condition: three or more planes intersecting along a common line.

Fig. 13 shows the singularity condition in case of two planes being coplanar. Similar to the first case, even when all actuators are locked, the moving platform cannot resist external moments that have components in the D_1D_3 direction. Point D_2 can momentarily move in the direction perpendicular to the planes. Fig. 14 shows the rare case where 4 planes intersect at a common point. At this configuration, one of the moving platform end-point will be at the intersection point (D_3 in this case). Even when all the actuator joints are locked, the moving platform will not be able to resist external moment about the vertical axis passing the intersection point which in this case is the intersection line of planes of Link-chain 1 and Link-chain 2. As shown in examples above, in the first type of singularity, the actuator momentarily cannot affect end-effector motion. This leads to end-effector being not completely controllable. The second type of singularity corresponds to the condition det(B)=0. This occurs when $\theta_{11} = \theta_{21}$, $\theta_{12} = \theta_{22}$ or $\theta_{13} = \theta_{23}$ which means l_{ln} and l_{un} are parallel.

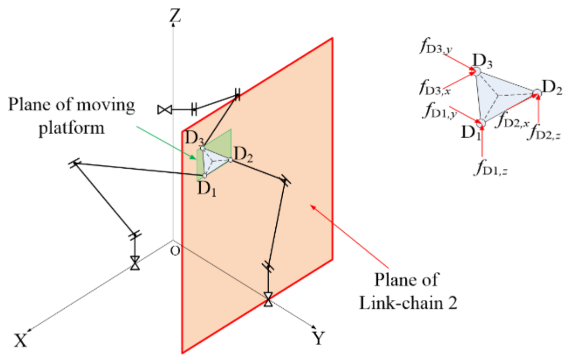

Fig.13. First type of singularity condition: two planes are coplanar.

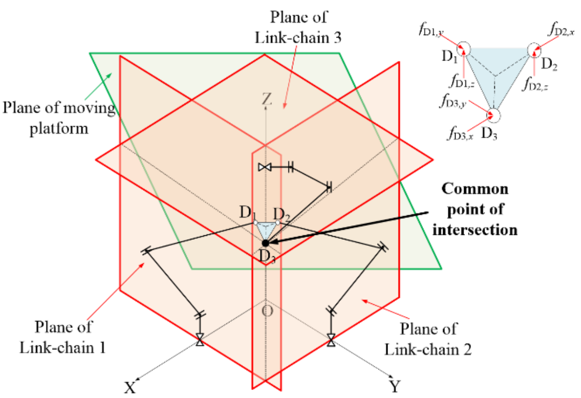

Fig.14. First type of singularity condition: four planes intersect at a common point.

In other words, the singularity of the second type occurs when one of the legs is either fully extended or the upper arm folds back directly on the lower arm. The degree of freedom in this type are decreased. As shown above, the geometrical approach allows us to visualize and foresee the singularity configuration of the robot at the design stage where no numerical values of robot parameters such as link length and distances are given. With the known singularity configurations, one can design robot parameter such as lengths and distance between legs to help avoid singularity condition. Alternatively, with a given set of robot parameters, one can choose the operating space to avoid singular configurations that exist within the system without checking the rank of Jacobian matrix in each grid points. This is an obvious advantage over the numerical approach.

CONCLUSION

There are only few studies on 6-DOF parallel robot with 3-leg structure. This study presents in-depth analysis on kinematic, workspace, and singularity of a particular type of parallel robot with 3-P$\overline{\mathrm{RR}}$S structure. Detailed solutions are provided. The inverse kinematic solutions can easily be obtained similar to most other parallel robot structures. The forward kinematic can be arranged to analytical form where solutions can be found using Dialytic elimination method. The number of solutions depends on length parameters of the robot. The minimum number of possible solutions is 1 and the maximum is 8. The workspace of the 3-P$\overline{\mathrm{RR}}$S robot can be determined geometrically by intersection of three tube-shape volumes formed from the reachable volume of each leg. Based on Grassmann-Cayley Algebra, four planes can be formed from the Jacobian matrix A. Based on the arrangement of these planes, three possible configurations correspond to the first type of singularity. The second type singularity occur when one or more legs is either fully extended or the upper arm folds back directly on the lower arm.

ACKNOWLEDGEMENT

This work was supported by Chiang Mai University's Mid-Career Grant 2014.

REFERENCES

Ben-Horin, P., and Shoham, M., "Singularity condition of six-degree-of-freedom three-legged parallel robot based on Grassmann-Cayley algebra,"; IEEE Transactions on Robotics, Vol. 20, No. 4, pp. 577-589 (2006).

Chen, C., Gayral, T., Caro, S., Chablat, D., Moroz, G., and Abeywardena, S., "A Six Degree of Freedom Epicyclic-Parallel Manipulator,"; Journal of Mechanisms and Robotics, Vol. 4, pp. 041011-1-041011-8 (2012).

Chifu, Y., Huang Q., Ogbobe, P.O., and Han, J., "Forward kinematic analysis of parallel robot using global newton-raphson method,"; In the Second International Conference on Intelligent Computation Technology and Automation, Changsha, Hunan, China (2009).

Gosselin C., and Angels, J., "Singularity analysis of closed-loop kinematic chains,"; IEEE Transactions on Robotics and Automation, Vol. 6, No. 3, pp. 284-290 (1990).

Gosselin, C., "Determination of the workspace of 6-6 dof parallel manipulator,"; ASME, J. of Mechanical Design, Vol. 112, No. 3, pp. 331-336 (1990).

Kai, L., Fitzgerald J. M., and Lewis, F. L., "Kinematic analysis of a Stewart platform manipulator,"; IEEE Transaction, Electronics, Vol. 40, No. 2, pp. 283-293 (1993).

Kefei, W., Taewon, S., and Lee, J.W., "A geometric approach for singularity analysis of 3-DOF planar parallel manipulators using Grassmann–Cayley algebra,”; *Robotica*, vol .35, no .3, pp .511-520, (2017).

Merlet, J. P., “Determination of 6D workspaces of Gough-type parallel manipulator and comparison between different geometries,”; The International Journal of Robotis Research, Vol. 18, No. 9, pp. 902-906 (1999).

Merlet, J. P., Parallel Robot (Solid mechanics and its application), 2nd ed., Springer-Verlag New York, USA, pp. 136–137 (2006).

Monsarrat, B. and Gosselin C., “Singularity analysis of a three-leg six-degree-of-freedom parallel platform structure based on Grassmann line geometry,”; The International Journal of Robotics Research, Vol. 20, No. 4, pp. 312-328 (2001).

Ping, J., and Houngtao, W., “A closed-form forward kinematics solution for 6-6 Stewart platform manipulator,”; IEEE Transaction Robotics and Automations, Vol. 17, No. 4, pp. 522-526 (2001).

Qian, Y., Wang, Q., Chen, G., Yu, J., and Cao, Y., “Workspace and singularity analysis of 3/3-RRRS parallel manipulator,”; Journal of Theoretical and Applied Information Technology, Vol. 48, No. 3, pp. 1423-1429 (2013).

Tongtib, A., Puangmali, P., and Wongratanaphisan, T., “Kinematic analysis of a 3-P$\overline{\text{RR}}$S parallel robot,”; In the 7th TSME International Conference on Mechanical Engineering, Chiang Mai, Thailand (2016).

Tsai, L. W., Robot analysis and design :The mechanics of serial and parallel manipulators, 1st ed., John Wiley & Sons, USA, 473–475 (1999).

Xiguang, H., and Guangpin, H. “Closed-form direct position analysis of the general Stewart-Gough manipulator robot,”; In the International Conference on Mechatronic and Automation, Changchun, China (2009).

APPENDIX

The symbolic forms of a_i

$$a_0=-d_1^8-d_2^8-d_3^8+8d_3^6D_{y1}^2-16d_3^4D_{x1}^2D_{y1}^2+32d_3^4D_{x1}D_{x3}D_{y1}^2-16d_3^4D_{x3}^2D_{y1}^2-16d_3^4D_{y1}^4-16d_3^6D_{y1}D_{y2}+32d_3^4D_{x1}^2D_{y1}D_{y2}-64d_3^4D_{x1}D_{x3}D_{y1}D_{y2}+32d_3^4D_{x3}^2D_{y1}D_{y2}+64d_3^4D_{y1}^3D_{y2}-16d_3^4D_{x1}^2D_{y2}^2+32d_3^4D_{x1}D_{x3}D_{y2}^2-16d_3^4D_{x3}^2D_{y2}^2+8d_3^6D_{y2}^2-96d_3^4D_{y1}^2D_{y2}^2+64d_3^4D_{y1}D_{y2}^3-8d_3^4D_{x1}^2D_{z2}^2-8d_3^4D_{x3}^2D_{z2}^2-32d_3^2D_{x1}^2D_{y1}^2D_{z2}^2+64d_3^2D_{x1}D_{x3}D_{y1}^2D_{z2}^2+16d_3^4D_{x1}D_{x3}D_{z2}^2-32d_3^2D_{x3}^2D_{y1}^2D_{z2}^2+64d_3^2D_{x1}^2D_{y1}D_{y2}D_{z2}^2+8d_3^6D_{z2}D_{z3}-128d_3^2D_{x1}D_{x3}D_{y1}D_{y2}D_{z2}^2-128d_3^2D_{x3}^2D_{y1}D_{y2}D_{z2}D_{z3}+64d_3^2D_{x3}^2D_{y1}D_{y2}D_{z2}^2+64d_3^4D_{y1}D_{y2}D_{z2}D_{z3}+32d_3^2D_{y1}^4D_{z3}^2-32d_3^2D_{x1}^2D_{y2}^2D_{z2}^2+64d_3^2D_{x1}D_{x3}D_{y2}^2D_{z2}^2-32d_3^2D_{x3}^2D_{y2}^2D_{z2}^2-16D_{x1}^4D_{z2}^4+64D_{x1}^3D_{x3}D_{z2}^4-96D_{x1}^2D_{x3}^2D_{z2}^4+64D_{x1}D_{x3}^3D_{z2}^4-16D_{x3}^4D_{z2}^4-32d_3^4D_{y1}^2D_{z2}D_{z3}+64d_3^2D_{x1}^2D_{y1}^2D_{z2}D_{z3}-128d_3^2D_{x1}D_{x3}D_{y1}^2D_{z2}D_{z3}+64d_3^2D_{x3}^2D_{y1}^2D_{z2}D_{z3}+32d_3^2D_{y1}^2D_{z2}^2D_{z3}^2-128d_3^2D_{x1}^2D_{y1}D_{y2}D_{z2}D_{z3}+256d_3^2D_{x1}D_{x3}D_{y1}D_{y2}D_{z2}D_{z3}-32d_3^4D_{y2}^2D_{z2}D_{z3}+64d_3^2D_{x1}^2D_{y2}^2D_{z2}D_{z3}+192d_3^2D_{y1}^2D_{y2}^2D_{z3}^2-128d_3^2D_{x1}D_{x3}D_{y2}^2D_{z2}D_{z3}+64d_3^2D_{x3}^2D_{y2}^2D_{z2}D_{z3}+32d_3^2D_{x1}^2D_{z2}^3D_{z3}-64d_3^2D_{x1}D_{x3}D_{z2}^3D_{z3}+32d_3^2D_{x3}^2D_{z2}^3D_{z3}-8d_3^4D_{y1}^2D_{z3}^2-32D_{x3}^2D_{y1}^2D_{z2}^2D_{z3}^2+16d_3^4D_{y1}D_{y2}D_{z3}^2-128d_3^2D_{y1}^3D_{y2}D_{z3}^2-8d_3^4D_{y2}^2D_{z3}^2-128d_3^2D_{y1}D_{y2}^3D_{z3}^2+64D_{x1}^2D_{y1}D_{y2}D_{z2}^2D_{z3}^2$$

$$+32d_3^2D_{y2}^4D_{z3}^2-24d_3^4D_{z2}^2D_{z3}^2-32D_{x1}^2D_{y1}^2D_{z2}^2D_{z3}^2-64d_3^2D_{y1}D_{y2}D_{z2}^2D_{z3}^2+64D_{x1}D_{x3}D_{y1}^2D_{z2}^2D_{z3}^2-128D_{x1}D_{x3}D_{y1}D_{y2}D_{z2}^2D_{z3}^2+64D_{x3}^2D_{y1}D_{y2}D_{z2}^2D_{z3}^2+32d_3^2D_{y2}^2D_{z2}^2D_{z3}^2-32D_{x1}^2D_{y2}^2D_{z2}^2D_{z3}^2+64D_{x1}D_{x3}D_{y2}^2D_{z2}^2D_{z3}^2-32D_{x3}^2D_{y2}^2D_{z2}^2D_{z3}^2-32D_{x1}^2D_{z2}^4D_{z3}^2+64D_{x1}D_{x3}D_{z2}^4D_{z3}^2-32D_{x3}^2D_{z2}^4D_{z3}^2+32d_3^2D_{y1}^2D_{z2}D_{z3}^3+64D_{y1}^3D_{y2}D_{z3}^4-64d_3^2D_{y1}D_{y2}D_{z2}D_{z3}^3+32d_3^2D_{y2}^2D_{z2}D_{z3}^3+32d_3^2D_{z2}^3D_{z3}^3-16D_{y1}^4D_{z3}^4-96D_{y1}^2D_{y2}^2D_{z3}^4+64D_{y1}D_{y2}^3D_{z3}^4-16D_{y2}^4D_{z3}^4-32D_{y1}^2D_{z2}^2D_{z3}^4+64D_{y1}D_{y2}D_{z2}^2D_{z3}^4-32D_{y2}^2D_{z2}^2D_{z3}^4-16D_{z2}^4D_{z3}^4+4d_2^6\{d_3^2-2D_{z2}D_{z3}\}+4d_1^6\{d_2^2-d_3^2+2\{D_{x1}^2-2D_{x1}D_{x3}+D_{x3}^2+D_{z2}D_{z3}\}\}+4d_2^2\{d_3^2-2D_{z2}D_{z3}\}\{d_3^4-4d_3^2\{D_{y1}^2-2D_{y1}D_{y2}+D_{y2}^2+D_{z2}D_{z3}\}+4\{D_{x1}^2\{2D_{y1}^2-4D_{y1}D_{y2}+2D_{y2}^2+D_{z2}^2\}-2D_{x1}D_{x3}\{2D_{y1}^2-4D_{y1}D_{y2}+2D_{y2}^2+D_{z2}^2\}+D_{x3}^2\{2D_{y1}^2-4D_{y1}D_{y2}+2D_{y2}^2+D_{z2}^2\}+\{D_{y1}^2-2D_{y1}D_{y2}+D_{y2}^2+D_{z2}^2\}D_{z3}^2\}\}-2d_2^4\{3d_3^4-4d_3^2\{D_{y1}^2-2D_{y1}D_{y2}+D_{y2}^2+3D_{z2}D_{z3}\}+4\{D_{x1}^2\{2D_{y1}^2-4D_{y1}D_{y2}+2D_{y2}^2+D_{z2}^2\}-2D_{x1}D_{x3}\{2D_{y1}^2-4D_{y1}D_{y2}+2D_{y2}^2+D_{z2}^2\}+D_{x3}^2\{2D_{y1}^2-4D_{y1}D_{y2}+2D_{y2}^2+D_{z2}^2\}+\{D_{y1}^2-2D_{y1}D_{y2}+D_{y2}^2+3D_{z2}^2\}D_{z3}^2\}\}-2d_1^4\{3d_2^4+3d_3^4-4d_3^2\{2D_{x1}^2-4D_{x1}D_{x3}+2D_{x3}^2+D_{y1}^2-2D_{y1}D_{y2}+D_{y2}^2+3D_{z2}D_{z3}\}+d_2^2\{-6d_3^2+8D_{x1}^2-16D_{x1}D_{x3}+8D_{x3}^2+12D_{z2}D_{z3}\}+4\{2D_{x1}^4-8D_{x1}^3D_{x3}+2D_{x3}^4+\{D_{y1}^2-2D_{y1}D_{y2}+D_{y2}^2+3D_{z2}^2\}D_{z3}^2+D_{x3}^2\{2D_{y1}^2-4D_{y1}D_{y2}+2D_{y2}^2+D_{z2}^2+4D_{z2}D_{z3}\}-2D_{x1}D_{x3}\{4D_{x3}^2+2D_{y1}^2-4D_{y1}D_{y2}+2D_{y2}^2+D_{z2}^2+4D_{z2}D_{z3}\}+D_{x1}^2\{12D_{x3}^2+2D_{y1}^2-4D_{y1}D_{y2}+2D_{y2}^2+D_{z2}^2+4D_{z2}D_{z3}\}\}\}+4d_1^2\{d_2^6-d_3^6+2d_3^4\{D_{x1}^2-2D_{x1}D_{x3}+D_{x3}^2+2D_{y1}^2-4D_{y1}D_{y2}+2D_{y2}^2+3D_{z2}D_{z3}\}+d_2^4\{-3d_3^2+2\{D_{x1}^2-2D_{x1}D_{x3}+D_{x3}^2+3D_{z2}D_{z3}\}\}-4d_3^2\{D_{x1}^2D_{z2}\{D_{z2}+2D_{z3}\}-2D_{x1}D_{x3}D_{z2}\{D_{z2}+2D_{z3}\}+D_{x3}^2D_{z2}\{D_{z2}+2D_{z3}\}+D_{z3}\{3D_{z2}^2D_{z3}+D_{y1}^2[2D_{z2}+D_{z3}]-2D_{y1}D_{y2}[2D_{z2}+D_{z3}]+D_{y2}^2[2D_{z2}+D_{z3}]\}\}+d_2^2\{3d_3^4-4d_3^2\{D_{x1}^2-2D_{x1}D_{x3}+D_{x3}^2+D_{y1}^2-2D_{y1}D_{y2}+D_{y2}^2+3D_{z2}D_{z3}\}+4\{[D_{y1}^2-2D_{y1}D_{y2}+D_{y2}^2+3D_{z2}^2]D_{z3}^2+D_{x1}^2[2D_{y1}^2-4D_{y1}D_{y2}+2D_{y2}^2+D_{z2}^2+2D_{z2}D_{z3}]-2D_{x1}D_{x3}[2D_{y1}^2-4D_{y1}D_{y2}+2D_{y2}^2+D_{z2}^2+2D_{z2}D_{z3}]+D_{x3}^2[2D_{y1}^2-4D_{y1}D_{y2}+2D_{y2}^2+D_{z2}^2+2D_{z2}D_{z3}]\}\}+8\{D_{x1}^4D_{z2}^2-4D_{x1}^3D_{x3}D_{z2}^2+D_{x3}^4D_{z2}^2+D_{z2}\{D_{y1}^2-2D_{y1}D_{y2}+D_{y2}^2+D_{z2}^2\}D_{z3}^3+D_{x3}^2D_{z3}\{D_{y1}^2[2D_{z2}-D_{z3}]+D_{y2}^2[2D_{z2}-D_{z3}]+2D_{y1}D_{y2}[-2D_{z2}+D_{z3}]+D_{z2}^2[D_{z2}+D_{z3}]\}-2D_{x1}D_{x3}\{2D_{x3}^2D_{z2}^2+D_{z3}[D_{y1}^2(2D_{z2}-D_{z3}(D_{y2}^2(2D_{z2}-D_{z3})+2D_{y1}D_{y2})-2D_{z2}+D_{z3})+D_{z2}^2(D_{z2}+D_{z3})]\}+D_{x1}^2\{6D_{x3}^2D_{z2}^2+D_{z3}[D_{y1}^2(2D_{z2}-D_{z3})+D_{y2}^2(2D_{z2}-D_{z3})+2D_{y1}D_{y2}(-2D_{z2}+D_{z3})+D_{z2}^2(D_{z2}+D_{z3})]\}\}\}\}$$

$$a_1=8\{\{-d_3^6\}D_{z2}+2d_3^4D_{x1}^2D_{z2}-4d_3^4D_{x1}D_{x3}D_{z2}+2d_3^4D_{x3}^2D_{z2}+4d_3^4D_{y1}^2D_{z2}-8d_3^4D_{y1}D_{y2}D_{z2}+4d_3^4D_{y2}^2D_{z2}-4d_3^2D_{x1}^2D_{z2}^3+8D_{x1}^4D_{z2}^3+8d_3^2D_{x1}D_{x3}D_{z2}^3-32D_{x1}^3D_{x3}D_{z2}^3-4d_3^2D_{x3}^2D_{z2}^3+48D_{x1}^2D_{x3}^2D_{z2}^3-32D_{x1}D_{x3}^3D_{z2}^3+8D_{x3}^4D_{z2}^3-d_3^6D_{z3}+6d_3^4D_{y1}^2D_{z3}-8d_3^2D_{x1}^2D_{y1}^2D_{z3}+16d_3^2D_{x1}D_{x3}D_{y1}^2D_{z3}-8d_3^2D_{x3}^2D_{y1}^2D_{z3}-8d_3^2D_{y1}^4D_{z3}+24d_3^2D_{x1}D_{x3}D_{z2}^2D_{z3}+6d_3^4D_{z2}^2D_{z3}-12d_3^4D_{y1}D_{y2}D_{z3}+16d_3^2D_{x1}^2D_{y1}D_{y2}D_{z3}-32d_3^2D_{x1}D_{x3}D_{y1}D_{y2}D_{z3}+16d_3^2D_{x3}^2D_{y1}D_{y2}D_{z3}+32d_3^2D_{y1}^3D_{y2}D_{z3}+6d_3^4D_{y2}^2D_{z3}-8d_3^2D_{x1}^2D_{y2}^2D_{z3}+16d_3^2D_{x1}D_{x3}D_{y2}^2D_{z3}-8d_3^2D_{x3}^2D_{y2}^2D_{z3}-48d_3^2D_{y1}^2D_{y2}^2D_{z3}+32d_3^2D_{y1}D_{y2}^3D_{z3}-8d_3^2D_{y2}^4D_{z3}-12d_3^2D_{x1}^2D_{z2}^2D_{z3}-12d_3^2D_{x3}^2D_{z2}^2D_{z3}-8d_3^2D_{y1}^2D_{z2}^2D_{z3}+8D_{x1}^2D_{y1}^2D_{z2}^2D_{z3}-16D_{x1}D_{x3}D_{y1}^2D_{z2}^2D_{z3}+8D_{x3}^2D_{y1}^2D_{z2}^2D_{z3}+16d_3^2D_{y1}D_{y2}D_{z2}^2D_{z3}+16D_{x1}^2D_{z2}^3D_{z3}^2-16D_{x1}^2D_{y1}D_{y2}D_{z2}^2D_{z3}+32D_{x1}D_{x3}D_{y1}D_{y2}D_{z2}^2D_{z3}-16D_{x3}^2D_{y1}D_{y2}D_{z2}^2D_{z3}-8d_3^2D_{y2}^2D_{z2}^2D_{z3}+8D_{x1}^2D_{y2}^2D_{z2}^2D_{z3}-16D_{x1}D_{x3}D_{y2}^2D_{z2}^2D_{z3}+8D_{x3}^2D_{y2}^2D_{z2}^2D_{z3}+8D_{x1}^2D_{z2}^4D_{z3}-16D_{x1}D_{x3}D_{z2}^4D_{z3}+8D_{x3}^2D_{z2}^4D_{z3}+6d_3^4D_{z2}D_{z3}^2-20d_3^2D_{y1}^2D_{z2}D_{z3}^2+8D_{x1}^2D_{y1}^2D_{z2}D_{z3}^2+16D_{x3}^2D_{z2}^3D_{z3}^2-16D_{x1}D_{x3}D_{y1}^2D_{z2}D_{z3}^2+8D_{x3}^2D_{y1}^2D_{z2}D_{z3}^2+40d_3^2D_{y1}D_{y2}D_{z2}D_{z3}^2-16D_{x1}^2D_{y1}D_{y2}D_{z2}D_{z3}^2+32D_{x1}D_{x3}D_{y1}D_{y2}D_{z2}D_{z3}^2-16D_{x3}^2D_{y1}D_{y2}D_{z2}D_{z3}^2-20d_3^2D_{y2}^2D_{z2}D_{z3}^2+8D_{x1}^2D_{y2}^2D_{z2}D_{z3}^2-16D_{x1}D_{x3}D_{y2}^2D_{z2}D_{z3}^2+8D_{x3}^2D_{y2}^2D_{z2}D_{z3}^2-12d_3^2D_{z2}^3D_{z3}^2-32D_{x1}D_{x3}D_{z2}^3D_{z3}^2-4d_3^2D_{y1}^2D_{z3}^3+8D_{y1}^4D_{z3}^3+8d_3^2D_{y1}D_{y2}D_{z3}^3-32D_{y1}^3D_{y2}D_{z3}^3-4d_3^2D_{y2}^2D_{z3}^3+48D_{y1}^2D_{y2}^2D_{z3}^3-32D_{y1}D_{y2}^3D_{z3}^3+8D_{y2}^4D_{z3}^3-12d_3^2D_{z2}^2D_{z3}^3+16D_{y1}^2D_{z2}^2D_{z3}^3-$$

$32D_{y1}D_{y2}D_{z2}^2D_{z3}^3+16D_{y2}^2D_{z2}^2D_{z3}^3+8D_{z2}^4D_{z3}^3+8D_{y1}^2D_{z2}D_{z3}^4-$
$16D_{y1}D_{y2}D_{z2}D_{z3}^4+8D_{y2}^2D_{z2}D_{z3}^4+8D_{z2}^3D_{z3}^4-d_1^6\{D_{z2}+D_{z3}\}$
$+d_2^6\{D_{z2}+D_{z3}\}+d_2^4\{-3d_3^2\{D_{z2}+D_{z3}\}+2\{D_{x1}^2D_{z2}-2D_{x1}D_{x3}D_{z2}$
$+D_{x3}^2D_{z2}+D_{z3}[D_{y1}^2-2D_{y1}D_{y2}+D_{y2}^2+3D_{z2}(D_{z2}+D_{z3})]\}\}+$
$d_1^4\{3d_2^2\{D_{z2}+D_{z3}\}-3d_3^2\{D_{z2}+D_{z3}\}+2\{D_{x1}^2[3D_{z2}+2D_{z3}]-$
$2D_{x1}D_{x3}[3D_{z2}+2D_{z3}]+D_{x3}^2[3D_{z2}+2D_{z3}]+D_{z3}[D_{y1}^2-2D_{y1}D_{y2}+$
$D_{y2}^2+3D_{z2}(D_{z2}+D_{z3})]\}\}+d_2^2\{3d_3^4\{D_{z2}+D_{z3}\}-4d_3^2\{D_{x1}^2D_{z2}-$
$2D_{x1}D_{x3}D_{z2}+D_{x3}^2D_{z2}+D_{y1}^2D_{z2}-2D_{y1}D_{y2}D_{z2}+D_{y2}^2D_{z2}+2D_{y1}^2D_{z3}-$
$4D_{y1}D_{y2}D_{z3}+2D_{y2}^2D_{z3}+3D_{z2}^2D_{z3}+3D_{z2}D_{z3}^2\}+4\{D_{z3}^2[3D_{z2}^2$
$(D_{z2}+D_{z3})+D_{y1}^2(3D_{z2}+D_{z3})-2D_{y1}D_{y2}(3D_{z2}+D_{z3})+$
$D_{y2}^2(3D_{z2}+D_{z3})]+D_{x1}^2[2D_{y1}^2(D_{z2}+D_{z3})-4D_{y1}D_{y2}(D_{z2}+D_{z3})$
$+2D_{y2}^2(D_{z2}+D_{z3})+D_{z2}^2(D_{z2}+3D_{z3})]-2D_{x1}D_{x3}[2D_{y1}^2(D_{z2}+D_{z3})-$
$4D_{y1}D_{y2}(D_{z2}+D_{z3})+2D_{y2}^2(D_{z2}+D_{z3})+D_{z2}^2(D_{z2}+3D_{z3})]+$
$D_{x3}^2[2D_{y1}^2(D_{z2}+D_{z3})-4D_{y1}D_{y2}(D_{z2}+D_{z3})+2D_{y2}^2(D_{z2}+D_{z3})+$
$D_{z2}^2(D_{z2}+3D_{z3})]\}\}-d_1^2\{3d_2^4\{D_{z2}+D_{z3}\}+3d_3^4\{D_{z2}+D_{z3}\}-$
$4d_3^2\{D_{y1}^2D_{z2}-2D_{y1}D_{y2}D_{z2}+D_{y2}^2D_{z2}+2D_{y1}^2D_{z3}-$
$4D_{y1}D_{y2}D_{z3}+2D_{y2}^2D_{z3}+3D_{z2}^2D_{z3}+3D_{z2}D_{z3}^2+D_{x1}^2[2D_{z2}+D_{z3}]-$
$2D_{x1}D_{x3}[2D_{z2}+D_{z3}]+D_{x3}^2[2D_{z2}+D_{z3}]\}+4\{2D_{x1}^4D_{z2}-$
$8D_{x1}^3D_{x3}D_{z2}+2D_{x3}^4D_{z2}+D_{x3}^2D_{z2}\{2D_{y1}^2-4D_{y1}D_{y2}+2D_{y2}^2+$
$D_{z2}^2+5D_{z2}D_{z3}+2D_{z3}^2\}-2D_{x1}D_{x3}D_{z2}\{4D_{x3}^2+2D_{y1}^2-4D_{y1}D_{y2}+$
$2D_{y2}^2+D_{z2}^2+5D_{z2}D_{z3}+2D_{z3}^2\}+D_{x1}^2D_{z2}\{12D_{x3}^2+2D_{y1}^2-$
$4D_{y1}D_{y2}+2D_{y2}^2+D_{z2}^2+5D_{z2}D_{z3}+2D_{z3}^2\}+D_{z3}^2\{3D_{z2}^2[D_{z2}+D_{z3}]+$
$D_{y1}^2[3D_{z2}+D_{z3}]-2D_{y1}D_{y2}[3D_{z2}+D_{z3}]+D_{y2}^2[3D_{z2}+D_{z3}]\}\}+$
$2d_2^2\{-3d_3^2\{D_{z2}+D_{z3}\}+2\{D_{x1}^2[2D_{z2}+D_{z3}]-2D_{x1}D_{x3}[2D_{z2}+D_{z3}]$
$+D_{x3}^2[2D_{z2}+D_{z3}]+D_{z3}[D_{y1}^2-2D_{y1}D_{y2}+D_{y2}^2+3D_{z2}(D_{z2}+D_{z3})]\}\}\}\}$

$a_2=-8\{-d_1^6+d_2^6-d_3^6+d_3^4D_{x1}^2-2d_3^4D_{x1}D_{x3}+d_3^4D_{x3}^2+5d_3^4D_{y1}^2-$
$4d_3^2D_{x1}^2D_{y1}^2+8d_3^2D_{x1}D_{x3}D_{y1}^2-4d_3^2D_{x3}^2D_{y1}^2-4d_3^2D_{y1}^4-$
$10d_3^4D_{y1}D_{y2}+8d_3^2D_{x1}^2D_{y1}D_{y2}+8d_3^2D_{x3}^2D_{y1}D_{y2}+16d_3^2D_{y1}^3D_{y2}+5$
$d_3^4D_{y2}^2-4d_3^2D_{x1}^2D_{y2}^2+8d_3^2D_{x1}D_{x3}D_{y2}^2-4d_3^2D_{x3}^2D_{y2}^2-$
$24d_3^2D_{y1}^2D_{y2}^2+16d_3^2D_{y1}D_{y2}^3-4d_3^2D_{y2}^4+3d_3^4D_{z2}^2+12D_{z2}^2D_{z3}^4-$
$12d_3^2D_{x1}^2D_{z2}^2+12D_{x1}^4D_{z2}^2+24d_3^2D_{x1}D_{x3}D_{z2}^2-48D_{x1}^3D_{x3}D_{z2}^2-$
$12d_3^2D_{x3}^2D_{z2}^2+72D_{x1}^2D_{x3}^2D_{z2}^2-48D_{x1}D_{x3}^3D_{z2}^2+12D_{x3}^4D_{z2}^2-$
$4d_3^2D_{y1}^2D_{z2}^2+4D_{x1}^2D_{y1}^2D_{z2}^2-16d_3^2D_{x1}D_{x3}D_{y1}D_{y2}+4D_{y2}^2D_{z3}^4-$
$8D_{x1}D_{x3}D_{y1}^2D_{z2}^2+4D_{x3}^2D_{y1}^2D_{z2}^2+8d_3^2D_{y1}D_{y2}D_{z2}^2+4D_{y1}^2D_{z3}^4-$
$8D_{x1}^2D_{y1}D_{y2}D_{z2}^2+16D_{x1}D_{x3}D_{y1}D_{y2}D_{z2}^2-8D_{x3}^2D_{y1}D_{y2}D_{z2}^2-$
$4d_3^2D_{y2}^2D_{z2}^2-8D_{x1}D_{x3}D_{y2}^2D_{z2}^2+4D_{x3}^2D_{y2}^2D_{z2}^2+4D_{x1}^2D_{z2}^4-$
$8D_{x1}D_{x3}D_{z2}^4+4D_{x3}^2D_{z2}^4+12d_3^4D_{z2}D_{z3}+4D_{x1}^2D_{y2}^2D_{z2}^2-$
$12d_3^2D_{x1}^2D_{z2}D_{z3}+24d_3^2D_{x1}D_{x3}D_{z2}D_{z3}-12d_3^2D_{x3}^2D_{z2}D_{z3}-$
$28d_3^2D_{y1}^2D_{z2}D_{z3}+16D_{x1}^2D_{y1}^2D_{z2}D_{z3}-12d_3^2D_{z2}^3D_{z3}-$
$32D_{x1}D_{x3}D_{y1}^2D_{z2}D_{z3}+16D_{x3}^2D_{y1}^2D_{z2}D_{z3}+56d_3^2D_{y1}D_{y2}D_{z2}D_{z3}-$
$32D_{x1}^2D_{y1}D_{y2}D_{z2}D_{z3}+64D_{x1}D_{x3}D_{y1}D_{y2}D_{z2}D_{z3}+12D_{z2}^4D_{z3}^2-$
$32D_{x3}^2D_{y1}D_{y2}D_{z2}D_{z3}-28d_3^2D_{y2}^2D_{z2}D_{z3}+16D_{x1}^2D_{y2}^2D_{z2}D_{z3}-$
$32D_{x1}D_{x3}D_{y2}^2D_{z2}D_{z3}+16D_{x3}^2D_{y2}^2D_{z2}D_{z3}+32D_{x1}^2D_{z2}^3D_{z3}-$
$64D_{x1}D_{x3}D_{z2}^3D_{z3}+32D_{x3}^2D_{z2}^3D_{z3}+3d_3^4D_{z3}^2-16d_3^2D_{y1}^2D_{z3}^2-$
$8D_{x1}D_{x3}D_{y1}^2D_{z3}^2+4D_{x3}^2D_{y1}^2D_{z3}^2+12D_{y1}^4D_{z3}^2+32d_3^2D_{y1}D_{y2}D_{z3}^2-$
$8D_{x1}^2D_{y1}D_{y2}D_{z3}^2+16D_{x1}D_{x3}D_{y1}D_{y2}D_{z3}^2-8D_{x3}^2D_{y1}D_{y2}D_{z3}^2-$
$48D_{y1}^3D_{y2}D_{z3}^2-16d_3^2D_{y2}^2D_{z3}^2+4D_{x1}^2D_{y2}^2D_{z3}^2+32D_{z2}^3D_{z3}^3-$
$8D_{x1}D_{x3}D_{y2}^2D_{z3}^2+4D_{x3}^2D_{y2}^2D_{z3}^2+24D_{y2}^2D_{z2}^2D_{z3}^2+72D_{y1}^2D_{y2}^2D_{z3}^2-$
$8D_{y1}D_{y2}D_{z3}^4+32D_{y1}^2D_{z2}D_{z3}^3+24D_{y1}^2D_{z2}^2D_{z3}^2-$
$12d_3^2D_{z2}D_{z3}^3+12D_{y2}^4D_{z3}^2-48D_{y1}D_{y2}D_{z2}^2D_{z3}^2+32D_{y2}^2D_{z2}D_{z3}^3-$
$48D_{y1}D_{y2}^3D_{z3}^2+24D_{x1}^2D_{z2}^2D_{z3}^2+24D_{x3}^2D_{z2}^2D_{z3}^2+4D_{x1}^2D_{y1}^2D_{z3}^2-$
$48D_{x1}D_{x3}D_{z2}^2D_{z3}^2-64D_{y1}D_{y2}D_{z2}D_{z3}^3-36d_3^2D_{z2}^2D_{z3}^2+d_2^4\{-$
$3d_3^2+D_{x1}^2-2D_{x1}D_{x3}+D_{x3}^2+12D_{z2}D_{z3}+3D_{z3}^2+D_{y2}^2+3D_{z2}^2-$
$2D_{y1}D_{y2}+D_{y1}^2\}+d_1^4\{D_{y1}^2+3d_2^2-3d_3^2+5D_{x1}^2-10D_{x1}D_{x3}+5D_{x3}^2-$
$2D_{y1}D_{y2}+D_{y2}^2+3D_{z2}^2+3D_{z3}^2\}-d_1^2\{3d_2^4+3d_3^4-6d_3^2\{D_{x1}^2+D_{y1}^2-$
$2D_{x1}D_{x3}+D_{x3}^2+D_{y2}^2-2D_{y1}D_{y2}+D_{z2}^2+4D_{z2}D_{z3}+D_{z3}^2\}+2d_2^2\{-$
$3d_3^2+3D_{x1}^2-6D_{x1}D_{x3}+3D_{x3}^2+3D_{z3}^2+D_{y1}^2+D_{y2}^2+3D_{z2}^2-$
$2D_{y1}D_{y2}+12D_{z2}D_{z3}\}+4\{D_{x1}^4+D_{x3}^4-4D_{x1}^3D_{x3}+D_{x3}^2[D_{y1}^2-$
$2D_{y1}D_{y2}+D_{y2}^2+4D_{z2}^2+7D_{z2}D_{z3}+D_{z3}^2]-2D_{x1}D_{x3}[2D_{x3}^2+D_{y1}^2-$
$2D_{y1}D_{y2}+D_{y2}^2+4D_{z2}^2+7D_{z2}D_{z3}+D_{z3}^2]+D_{x1}^2[6D_{x3}^2+D_{y1}^2-$
$2D_{y1}D_{y2}+D_{y2}^2+4D_{z2}^2+7D_{z2}D_{z3}+D_{z3}^2]+3D_{z3}[D_{y1}^2(D_{z2}+D_{z3})-$
$2D_{y1}D_{y2}(D_{z2}+D_{z3})+D_{y2}^2(D_{z2}+D_{z3})+D_{z2}(D_{z2}^2+3D_{z2}D_{z3}+D_{z3}^2)]\}\}+$
$d_2^2\{3d_3^4-2d_3^2\{D_{x1}^2-2D_{x1}D_{x3}+D_{x3}^2+3[D_{y1}^2-2D_{y1}D_{y2}+$
$D_{y2}^2+4D_{z2}D_{z3}+D_{z3}^2+D_{z2}^2]\}+4\{D_{x1}^2[2D_{y1}^2+2D_{y2}^2+3D_{z2}$
$(D_{z2}+D_{z3})-4D_{y1}D_{y2}]-2D_{x1}D_{x3}[3D_{z2}(D_{z2}+D_{z3})+2D_{y2}^2+$
$2D_{y1}^2-4D_{y1}D_{y2}]+D_{x3}^2[2D_{y1}^2+2D_{y2}^2+3D_{z2}(D_{z2}+D_{z3})-4D_{y1}$
$D_{y2}]+3D_{z3}[D_{y1}^2(D_{z2}+D_{z3})-2D_{y1}D_{y2}+D_{z2}(D_{z2}^2+3D_{z2}D_{z3}$
$+D_{z3}^2)]\}\}\}$

$a_3=16\{3d_3^4D_{z2}-6d_3^2D_{x1}^2D_{z2}+4D_{x1}^4D_{z2}+12d_3^2D_{x1}D_{x3}D_{z2}-$
$16D_{x1}^3D_{x3}D_{z2}-6d_3^2D_{x3}^2D_{z2}+24D_{x1}^2D_{x3}^2D_{z2}-10d_3^2D_{y1}^2D_{z3}-$
$16D_{x1}D_{x3}^3D_{z2}+4D_{x3}^4D_{z2}-6d_3^2D_{y1}^2D_{z2}+4D_{x1}^2D_{y1}^2D_{z2}-$
$8D_{x1}D_{x3}D_{y1}^2D_{z2}+4D_{x3}^2D_{y1}^2D_{z2}+12d_3^2D_{y1}D_{y2}D_{z2}-$
$8D_{x1}^2D_{y1}D_{y2}D_{z2}+16D_{x1}D_{x3}D_{y1}D_{y2}D_{z2}-8D_{x3}^2D_{y1}D_{y2}D_{z2}-$
$6d_3^2D_{y2}^2D_{z2}+4D_{x1}^2D_{y2}^2D_{z2}-8D_{x1}D_{x3}D_{y2}^2D_{z2}+4D_{x3}^2D_{y2}D_{z2}-$
$2d_3^2D_{z2}^3+8D_{x1}^2D_{z2}D_{z2}^3-16D_{x1}D_{x3}D_{z2}^3+8D_{x3}^2D_{z2}^3+3d_3^4D_{z3}-$
$2d_3^2D_{x1}^2D_{z3}+4d_3^2D_{x1}D_{x3}D_{z3}-2d_3^2D_{x3}^2D_{z3}+4D_{x1}^2D_{y1}^2D_{z3}-$
$8D_{x1}D_{x3}D_{y1}^2D_{z3}+4D_{x3}^2D_{y1}^2D_{z3}+4D_{y1}^4D_{z3}+20d_3^2D_{y1}D_{y2}D_{z3}-$
$8D_{x1}^2D_{y1}D_{y2}D_{z3}+16D_{x1}D_{x3}D_{y1}D_{y2}D_{z3}-8D_{x3}^2D_{y1}D_{y2}D_{z3}-$
$16D_{y1}^3D_{y2}D_{z3}-10d_3^2D_{y2}^2D_{z3}+4D_{x1}^2D_{y2}^2D_{z3}+8D_{x1}^2D_{z2}D_{z3}^2-$
$8D_{x1}D_{x3}D_{y2}^2D_{z3}+4D_{x3}^2D_{y2}^2D_{z3}+24D_{y1}^2D_{y2}^2D_{z3}+8D_{y1}^2D_{z3}^3-$
$16D_{y1}D_{y2}^3D_{z3}+4D_{y2}^4D_{z3}-18d_3^2D_{z2}^2D_{z3}+24D_{x1}^2D_{z2}^2D_{z3}-$
$48D_{x1}D_{x3}D_{z2}^2D_{z3}+24D_{x3}^2D_{z2}^2D_{z3}+8D_{y1}^2D_{z2}^2D_{z3}+4D_{z2}D_{z3}^4-$
$16D_{y1}D_{y2}D_{z2}^2D_{z3}+8D_{y2}^2D_{z2}^2D_{z3}+4D_{z2}^4D_{z3}-18d_3^2D_{z2}D_{z3}^2-$
$16D_{x1}D_{x3}D_{z2}D_{z3}^2+8D_{x3}^2D_{z2}D_{z3}^2+24D_{y1}^2D_{z2}D_{z3}^2+24D_{z2}^2D_{z3}^3-$
$48D_{y1}D_{y2}D_{z2}D_{z3}^2+24D_{y2}^2D_{z2}D_{z3}^2+24D_{z2}^3D_{z3}^2-2d_3^2D_{z3}^3-$
$16D_{y1}D_{y2}D_{z3}^3+8D_{y2}^2D_{z3}^3+3d_1^4[D_{z2}+D_{z3}]+3d_2^4[D_{z2}+D_{z3}]-$
$2d_1^2[5D_{x1}^2D_{z2}-2D_{y1}D_{y2}D_{z2}+3D_{x1}^2D_{z3}-10D_{x1}D_{x3}D_{z3}+5D_{x3}^2D_{z2}-$
$6D_{x1}D_{x3}D_{z2}+3D_{y1}^2D_{z3}+3D_{x3}^2D_{z3}+D_{y1}^2D_{z2}+D_{y2}^2D_{z2}+D_{z2}^3-$
$6D_{y1}D_{y2}D_{z3}+3D_{y2}^2D_{z3}+9D_{z2}^2D_{z3}+9D_{z2}D_{z3}^2+D_{z3}^3+3d_2^2(D_{z2}+$
$D_{z3})-3d_3^2(D_{z2}+D_{z3})]+2d_2^2[3D_{x3}^2D_{z2}+D_{y1}^2D_{z2}+3D_{y2}^2D_{z3}-$
$2D_{y1}D_{y2}D_{z2}+D_{y2}^2D_{z2}+D_{z2}^3+D_{x3}^2D_{z3}+3D_{y1}^2D_{z3}+9D_{z2}^2D_{z3}-$
$6D_{y1}D_{y2}D_{z3}+9D_{z2}D_{z3}^2+D_{z3}^3D_{x1}^2(3D_{z2}+D_{z3})-2D_{x1}D_{x3}(3D_{z2}+D_{z3})]\}$

$a_4=-8\{3d_1^4+3d_2^4+3d_3^4-4d_3^2D_{x1}^2+2D_{x1}^4+8d_3^2D_{x1}D_{x3}-4d_3^2D_{x3}^2-$
$8D_{x1}^3D_{x3}+12D_{x1}^2D_{x3}^2-8D_{x1}D_{x3}^3+2D_{x3}^4-8d_3^2D_{y1}^2+4D_{x1}^2D_{y1}^2-$
$8D_{x1}D_{x3}D_{y1}^2+4D_{x3}^2D_{y1}^2+2D_{y1}^4+16d_3^2D_{y1}D_{y2}-$
$8D_{x1}^2D_{y1}D_{y2}+16D_{x1}D_{x3}D_{y1}D_{y2}-8D_{x3}^2D_{y1}D_{y2}-8D_{y1}^3D_{y2}-$
$8d_3^2D_{y2}^2+4D_{x1}^2D_{y2}^2-8D_{x1}D_{x3}D_{y2}^2+4D_{x3}^2D_{y2}^2+12D_{y1}^2D_{y2}^2-$
$8D_{y1}D_{y2}^3+2D_{y2}^4+2D_{z3}^4-12d_3^2D_{z2}^2+24D_{x1}^2D_{z2}^2-48D_{x1}D_{x3}D_{z2}^2$
$+24D_{x3}^2D_{z2}^2+4D_{y1}^2D_{z2}^2-8D_{y1}D_{y2}D_{z2}^2+4D_{y2}^2D_{z2}^2-$
$36d_3^2D_{z2}D_{z3}+32D_{x1}^2D_{z2}D_{z3}-64D_{x1}D_{x3}D_{z2}D_{z3}+32D_{x3}^2D_{z2}D_{z3}+$
$32D_{y1}^2D_{z2}D_{z3}+4D_{x3}^2D_{z3}^2-64D_{y1}D_{y2}D_{z2}D_{z3}+32D_{z2}^3D_{z3}-$
$12d_3^2D_{z3}^2+4D_{x1}^2D_{z3}^2+2D_{z2}^4-8D_{x1}D_{x3}D_{z3}^2+32D_{y2}^2D_{z2}D_{z3}+$
$32D_{z2}D_{z3}^3+24D_{y2}^2D_{z3}^2-48D_{y1}D_{y2}D_{z3}^2+72D_{z2}^2D_{z3}^2+d_2^2[-$
$6d_3^2+4(D_{x1}^2+D_{x3}^2+D_{y1}^2-2D_{y1}D_{y2}+D_{y2}^2+3D_{z2}^2+9D_{z2}D_{z3}+$
$3D_{z3}^2-2D_{x1}D_{x3})]-2d_1^2[3d_2^2-3d_3^2+2(2D_{x1}^2-4D_{x1}D_{x3}+2D_{x3}^2$
$+D_{y1}^2+9D_{z2}D_{z3}+3D_{z3}^2-2D_{y1}D_{y2}+3D_{z2}^2+D_{y2}^2)]\}$

$a_5=-32[3d_3^2D_{z2}-4D_{x1}^2D_{z2}+8D_{x1}D_{x3}D_{z2}-2D_{y1}^2D_{z2}+3d_3^2D_{z3}-$
$4D_{x3}^2D_{z2}+4D_{y1}D_{y2}D_{z2}-2D_{y2}^2D_{z2}-2D_{z2}^3-2D_{x1}^2D_{z3}-2D_{x3}^2D_{z3}-$
$4D_{y1}^2D_{z3}+8D_{y1}D_{y2}D_{z3}-4D_{y2}^2D_{z3}-12D_{z2}^2D_{z3}-12D_{z2}D_{z3}^2-$
$2D_{z3}^3+4D_{x1}D_{x3}D_{z3}+3d_1^2(D_{z2}+D_{z3})-3d_2^2(D_{z2}+D_{z3})]$

$a_6=32(d_1^2-d_2^2+d_3^2-D_{x1}^2+2D_{x1}D_{x3}-D_{x3}^2-D_{y1}^2+2D_{y1}D_{y2}-D_{y2}^2-$
$3D_{z2}^2-8D_{z2}D_{z3}-3D_{z3}^2)$

$a_7=64(D_{z2}+D_{z3})$

$a_8=-16$